

# Measurements of the three-dimensional scalar dissipation rate in gas-phase planar turbulent jets

By L. K. Su

## 1. Motivation and objectives

The scalar dissipation rate,  $\chi \equiv D\nabla C \cdot \nabla C$ , where  $C$  is a conserved scalar and  $D$  is the scalar diffusivity, is a quantity which is of great interest to models of turbulent non-premixed combustion. Mathematically, it represents the loss term in the evolution equation for  $\frac{1}{2}C^2$ , the scalar energy:

$$\left( \frac{\partial}{\partial t} + \mathbf{u} \cdot \nabla - D\nabla^2 \right) \frac{1}{2}C^2 = -D\nabla C \cdot \nabla C \equiv -\chi.$$

Physically,  $\chi$  can be interpreted as a mixing rate, or equivalently as a rate at which scalar fluctuations are destroyed. More specifically for combustion applications, Peters (1983) identified  $\chi$  as a characteristic diffusion time scale, imposed by the mixing field. Then, local flame extinction could be explained by the scalar dissipation rate exceeding a critical value, thus making the diffusion time smaller than the chemical time of the local flame structure. Accurate representation of flame quenching and stabilization poses notable difficulties for diffusion flame computations, because the scalar dissipation can occur at the finest mixing length scales of the flow. This means that modeling is required for the scalar dissipation in, for example, large-eddy simulations (LES) of turbulent combustion, where the filtered mixture fraction is used as a starting point to describe the combustion.

This study will address two issues regarding the properties of the scalar dissipation which are of particular significance in the context of combustion. The first concerns the length scales at which dissipation occurs, in particular their magnitude and their dependence on Reynolds number. The second issue concerns the scaling of the mean dissipation values with downstream distance in jet flows. Defining the thicknesses of the dissipation layers will be of use in determining the resolution requirements of both DNS and LES computations of turbulent diffusion flames. Meanwhile, experimental assessment of existing models for the downstream decay of mean dissipation will provide a fundamental test of our understanding of the properties of the dissipation rate.

The experimental data used in this study are the planar measurements of the complete, three-dimensional scalar dissipation rate by Su & Clemens (1998a,b) in the self-similar region of a gas-phase planar turbulent jet. The data are unique in providing scalar field information simultaneously in two parallel spatial planes, with sufficient resolution to permit differentiation in all three spatial dimensions. Determining the three spatial components explicitly obviates the need to invoke Taylor's hypothesis, while the planar nature of the measurement volume allows direct determination of structural properties of the dissipation field.

Previous planar measurements of the three-dimensional scalar dissipation at the smallest scales have been demonstrated in water flows (Southerland & Dahm (1994)). Some difficulties may arise, however, in applying scalar mixing results in the liquid phase to the gas phase, which is of particular interest in combustion applications. The Schmidt number ( $Sc \equiv \nu/D$ , where  $\nu$  is the kinematic viscosity and  $D$  the molecular diffusivity) of water is approximately 2000, while in gas-phase flows  $Sc \approx 1$ . From Batchelor (1952), the ratio of the smallest length scales in the velocity and scalar gradient fields in turbulent mixing scales as  $Sc^{-1/2}$ . Thus, while in water flows scalar gradients can be sustained on scales roughly 45 times smaller than the smallest velocity gradient scales, in the gas phase these scales are expected to be of the same order. It is reasonable to expect that the details of scalar mixing in the high and low Schmidt number regimes will differ as a result. Results from analysis of the present gas-phase scalar dissipation data are expected to be directly applicable to mixing in combustion systems.

### 1.1 Expressions for the dissipation length scale

Some confusion arises in defining the dissipation length scale in turbulent flows because different expressions are used. Here we will define the scalar dissipation length scale as

$$\lambda_D = \Lambda \delta Re_\delta^{-3/4} Sc^{-1/2}, \quad (1)$$

where  $\delta$  is the flow width,  $Re_\delta$  is the Reynolds number based on  $\delta$  and a measure of large-scale velocity,  $Sc$  is the Schmidt number, and the constant  $\Lambda$  is to be determined. More commonly, this dissipation scale is expressed in the form due to Kolmogorov and Batchelor. From dimensional arguments, Kolmogorov showed that the finest turbulence length scale,  $\lambda_K$ , should depend on the kinematic viscosity,  $\nu$ , and mean kinetic energy dissipation rate,  $\epsilon$ , as

$$\lambda_K \equiv (\nu^3/\epsilon)^{1/4}. \quad (2)$$

Subsequently, Batchelor introduced the equivalent expression for the scalar dissipation length scale,

$$\lambda_B \equiv \lambda_K \cdot Sc^{-1/2}.$$

The expressions for  $\lambda_D$  and  $\lambda_B$  are equivalent to within a constant factor. To show this, begin by expressing the mean kinetic energy dissipation as  $\epsilon \propto U^3/\delta$ , where  $U$  and  $\delta$  respectively are measures of the large-scale velocity and flow width. In the self-similar region of a round jet, Friehe *et al.* (1971) found

$$\epsilon = 48 \frac{U_0^3}{d} \left(\frac{y}{d}\right)^{-4},$$

where  $y$  is the downstream coordinate,  $U_0$  the initial jet velocity, and  $d$  the jet nozzle diameter. To convert to the large-scale variables  $U$  and  $\delta$ , we use the relations  $U/U_0 = 6.2(y/d)^{-1}$  and  $\delta = 0.37y$  (e.g. Chen & Rodi (1980)), defining  $U$  as the jet

mean centerline velocity and  $\delta$  as the jet full-width at the 5% points of the velocity profile. Then, Friehe's result becomes

$$\epsilon = 0.075 \left( \frac{U^3}{\delta} \right).$$

Though derived from results for the round jet, this result should be general to all turbulent shear flows, under the assumption that the small-scale behavior of fully developed turbulence is universal and is described by the parameters  $U$  and  $\delta$ .

Inserting this result for  $\epsilon$  into the definition for  $\lambda_B$ , and using  $Re_\delta \equiv U\delta/\nu$ , we obtain

$$\lambda_B = 0.075^{-1/4} \delta \left( \frac{\nu^3}{U^3 \delta^3} \right)^{1/4} Sc^{-1/2} = 1.9 \delta \cdot Re_\delta^{-3/4} Sc^{-1/2}. \quad (3)$$

Thus the Batchelor scale  $\lambda_B$  is equivalent to  $\lambda_D$  with a coefficient  $\Lambda = 1.9$ . The coefficient 1.9 appearing in these relations results from assuming a proportionality constant of 1 in the Kolmogorov/Batchelor scale definition. Since that definition is purely dimensional, there is no reason to expect that the proper proportionality constant should be 1. Empirical determination of the true value for  $\Lambda$  is discussed below (Section 2.2.1).

## 2. Accomplishments

### 2.1 Experimental conditions

This section presents a brief discussion of the experimental method. A comprehensive description can be found in Su & Clemens (1998a,b).

#### 2.1.1 Flow field

The flow considered in these experiments is a planar, turbulent jet of propane issuing into a slow co-flow of air. The nozzle exit has a slot width  $h = 1$  mm and spans 150 mm. This aspect ratio is sufficiently high that three-dimensional effects in the mean flow should be negligible in the flow region of interest, which extends to  $127h$  downstream of the exit. The nozzle itself has a contraction ratio of 75 : 1 to provide a uniform exit velocity profile. Jet exit velocities ranged from 5.9 to 10.7 m/s, while the co-flow velocity was 0.3 m/s. For the planar jet, the jet exit Reynolds number is insufficient to describe the local turbulence because the centerline velocity decays as  $y^{-1/2}$  ( $y$  is the downstream coordinate) while the jet grows linearly in  $y$ , so the local outer scale Reynolds number,  $Re_\delta$ , grows as  $y^{1/2}$ . Here,  $Re_\delta$  was determined using the scalings of Bradbury (1965) and Everitt & Robins (1978), namely

$$\delta_{0.05} = 0.39 y \quad (4)$$

and

$$U/U_0 = 2.4 (\rho_J/\rho_\infty)^{1/2} (y/h)^{-1/2},$$

and using the kinematic viscosity of air,  $\nu = 0.155 \text{ cm}^2/\text{s}$ . For the present measurements, consisting of a total of 906 image pairs,  $y$  ranged from 65 to  $127h$ , and  $Re_\delta$  ranged from 3200 to 8400. The binary diffusivity of propane and air is  $D = 0.114 \text{ cm}^2/\text{s}$ , giving a Schmidt number of 1.36.

### 2.1.2 Laser diagnostics

Previous efforts at three-dimensional scalar field imaging in gas-phase flows have used either simultaneous two-plane Rayleigh scattering (Yip & Long (1986)), or multi-plane scattering or laser-induced fluorescence (LIF), in which a single laser sheet is swept through a three-dimensional volume (Yip *et al.* (1988)). The former measurements, however, showed somewhat weak signal levels, while the latter technique suffers from temporal resolution limitations introduced by the laser sheet scanning.

The current measurements were performed by simultaneous Rayleigh scattering and LIF in two planes. This approach eliminates temporal skewing effects, while the high efficiency of LIF yields much higher signal levels for a given amount of laser energy than two-plane Rayleigh scattering. In fact, only a single, frequency-doubled Nd:YAG laser was required. Propane was chosen for the jet fluid because its high index of refraction results in a Rayleigh scattering cross-section over 13 times that of air. For the LIF, acetone was seeded into the jet fluid to approximately 5% by volume. The 532 nm output of the laser was split so that 75% was used for the Rayleigh scattering, while the remainder was further doubled to 266 nm to excite the LIF. The resulting laser sheet energies were typically 240 mJ/pulse at 532 nm and 30 mJ/pulse at 266 nm. To capture the signals, two slow-scan, thermoelectrically cooled CCD cameras, with  $500 \times 500$  pixel resolution, were used. Optical filters ensured separation of the LIF signal (which peaks in the range 400-500 nm) from the 532 nm Rayleigh scattering signal. To obtain the scalar concentrations from the raw imaging signals, standard background and sheet intensity profile corrections were performed. For additional accuracy, however, the intensity profiles for the two sheets were captured for individual pulses rather than on an average basis.

In computing the three components  $\partial C/\partial x_i$  of the scalar gradient vector, the out-of-plane component (here,  $\partial C/\partial z$ ) will be subject to the highest uncertainties, owing to the need to perform the difference calculation across distinct planes, which were obtained by different techniques and processed independently. To quantify the errors incurred, Su & Clemens (1998a,b) applied the two-plane technique to a single spatial plane, for which the scalar fields measured in the two imaging planes should be equal. Deviations from this were used to estimate the errors in the three-dimensional measurements. It was found that errors in the  $\partial C/\partial z$  term were substantially smaller than the magnitudes of  $\partial C/\partial z$  corresponding to significant events in the dissipation fields.

### 2.1.3 Spatial resolution

To increase signal levels, the scalar field images were binned  $2 \times 2$ ; in the data reduction process it was also necessary to match the fields of view of the two cameras geometrically, with the resulting pixel resolution being  $220 \times 220$ . This measurement area spanned 34 jet widths,  $h$ , per side, giving a grid resolution  $\Delta x = \Delta y$  of roughly  $150 \mu\text{m}$ . The 266 nm laser sheet showed a Gaussian cross-sectional profile, with a full width at the 5% points of  $200 \mu\text{m}$  at its waist, while the 532 nm laser sheet showed a roughly uniform profile with a full width of  $180 \mu\text{m}$ . The laser sheet spacing  $\Delta z$  was  $200 \mu\text{m}$ . These parameters are to be compared with the estimated finest

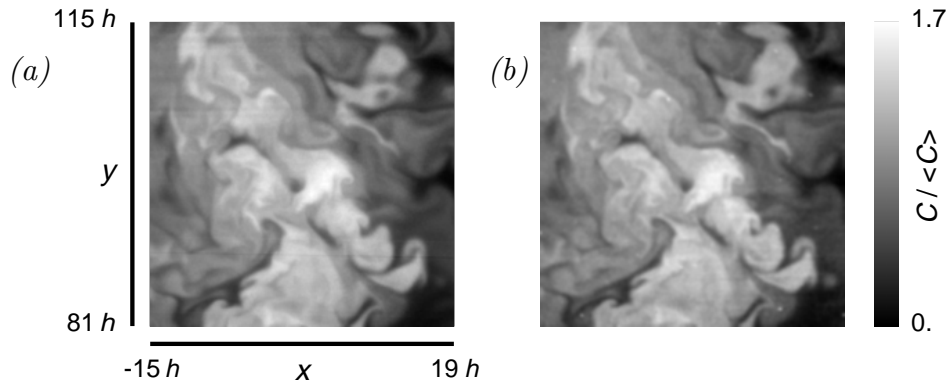


FIGURE 1. Scalar fields measured by (a) PLIF and (b) Rayleigh scattering, with a laser sheet separation of  $200 \mu\text{m}$ . The mean flow direction is upward in the images. The Reynolds number,  $Re_\delta$ , evolves from 5100 to 6200 in the measurement area.

dissipation length scale  $\lambda_D$  (Eq. 1), here computed using  $\Lambda = 11.2$  as suggested by Buch & Dahm (1991). For these measurements the downstream coordinate  $y$  spanned from  $65$  to  $127 h$ , and the Reynolds number  $Re_\delta$  ranged from  $3200$  to  $8400$ . The resulting  $\lambda_D$  ranged from  $370 \mu\text{m}$  to  $720 \mu\text{m}$ . Therefore  $0.21 < \Delta x / \lambda_D < 0.41$  and  $0.28 < \Delta z / \lambda_D < 0.54$ , where these non-dimensional grid spacings should be  $0.5$  or less to satisfy the Nyquist resolution criterion.

## 2.2 Results

A scalar field image pair obtained by this simultaneous Rayleigh/LIF technique is shown in Fig. 1. The mean flow is upward in the images, so the positive  $y$  direction is streamwise, while the  $x$  direction is cross-span and the  $z$  (out-of-plane) direction is spanwise relative to the mean flow. In these fields  $C$  is normalized by  $\langle C \rangle$ , the mean centerline concentration value for the full set of 906 image pairs.

Figure 2a shows the scalar dissipation for the scalar field of Fig. 1. The in-plane derivative components were determined from the LIF image (Fig. 1a) by two-point central differencing, and the out-of-plane component was found by simple differencing between the LIF and Rayleigh images. The dissipation shown in the figure is non-dimensional, with the scalar values being normalized by  $\langle C \rangle$ , and the  $\Delta x_i$  used in the differencing being normalized by  $\lambda_D$  (Eq. 1), with  $\Lambda = 11.2$ . Figure 2b shows the dissipation layer centers for dissipation field of Fig. 2a. The layer center field was compiled by first identifying peaks in the dissipation field. A given point was determined to be a ‘peak’ if it both exceeded a given threshold, and represented the local maximum of dissipation in both its positive and negative in-plane scalar gradient directions. A connectivity condition was then imposed on the peak field to remove noise effects. For Fig. 2a, the threshold value was that which captures 50% of the total dissipation for the full data set (non-dimensional  $\chi = 0.058$ ), and the connectivity condition required that the dissipation structures span a minimum length of twice  $\lambda_D$ .

The probability distribution of the logarithm of the dissipation is shown in Fig. 3. Also shown is a Gaussian distribution having the same first two moments. The

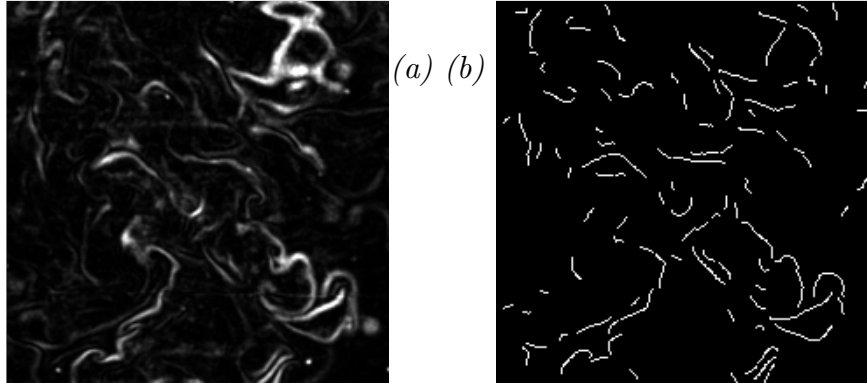


FIGURE 2. (a) The non-dimensional scalar dissipation for the scalar fields of Fig. 1. (b) The layer centers.

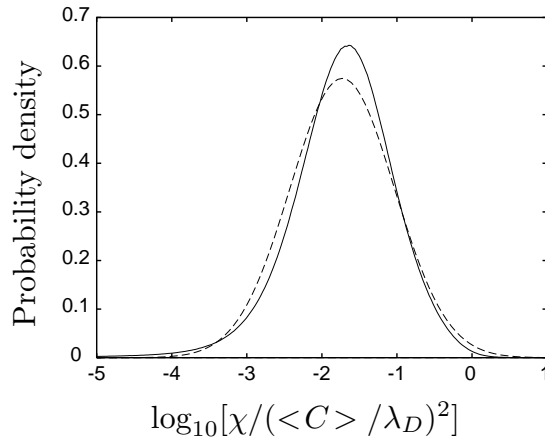


FIGURE 3. Distribution of the logarithm of the non-dimensional scalar dissipation. Current data, —; Gaussian (with same first two moments), ----.

measured distribution follows the Gaussian quite closely, except for a slight negative skewness. Similar asymmetry has been observed in both experiments (Feikema et al. (1996)) and direct numerical simulations (Eswaran & Pope (1988)) of scalar mixing, and has also been seen in the kinetic energy dissipation in DNS (Vincent & Meneguzzi (1991)).

### 2.2.1 Length scales

It is generally accepted that the scalar dissipation field is organized into layers; the thickness of these layers will scale with the local outer scale Reynolds number,  $Re_\delta$ , in a manner dependent on the strain field on the layers. Where the strain field is the inner scale strain the normalized layer thickness,  $\lambda_D/\delta$ , scales as  $Re_\delta^{-3/4}$  (Batchelor/Kolmogorov scaling), while if the strain field were the outer scale strain the thickness would scale as  $Re_\delta^{-1/2}$  (Taylor scaling). The traditional view (e.g. Tennekes & Lumley (1972)) holds that the bulk of the scalar dissipation occurs at the Batchelor scale, though Dowling (1991), based on time-resolved single point scalar

field measurements, has suggested that the regions of highest dissipation observe Taylor scaling. Nevertheless, Dowling (1991) found that the smallest dissipation scales observe Batchelor scaling.

Numerous studies have attempted to find the value of the constant  $\Lambda$  in Eq. 1 which accurately defines the size of the smallest dissipation scales. These efforts have generally proceeded by analysis of single-point scalar or velocity time series data. The difficulties of this approach can be seen by noting that Dowling & Dimotakis (1990) found  $\Lambda \approx 25$  from spectra of scalar concentration fluctuations, while, using the same scalar time series data set, Dowling (1991) subsequently obtained  $\Lambda \approx 5$  from scalar dissipation rate estimates. In contrast, Buch & Dahm (1991) determined  $\Lambda = 11.2$  from explicit measurement of the average thicknesses of dissipation structures in two-dimensional scalar field images. This latter approach is taken here.

Consistent with Buch & Dahm (1991), we define  $\lambda_D$  from Eq. 1 as the average of the full widths of the dissipation layers, where this width is computed as the distance across a layer between those points where the dissipation is 20% of the maximum. As a first step in computing the layer thicknesses, the layer center fields for the images were found, as described in Sec. 2.2 and shown in Fig. 2b. For each of the points on these layer centers, a search was then performed in the scalar gradient direction (both positive and negative) until the dissipation value dropped to 20% of the maximum. The resulting layer half width values were then doubled to give a measure of the full width. Statistics were not compiled for those layers where the dissipation failed to drop monotonically, indicating a possible intersection of layers. Finally, because the dissipation images, and thus the thickness computations, are strictly two-dimensional, the resulting thicknesses were adjusted by a factor of  $\cos \phi$ , where  $\phi$  is the out-of-plane angle of  $\nabla C$ .

Figure 4 shows the distribution of layer thicknesses, expressed in terms of  $\Lambda$ , as determined from Eq. 1. The threshold and connectivity conditions used for the layer center determination were the same as those used to compute the layer center field of Fig. 2b. To minimize the effect of the  $\cos \phi$  correction, only dissipation maxima where  $\phi \leq 60^\circ$  were considered. The mean of the distribution is  $\Lambda = 14.8$ , indicating the the layers in these data are somewhat thicker than predicted by Buch & Dahm (1991), and are over seven times larger than the Batchelor scale determined using a proportionality constant of 1 in the Kolmogorov scale definition (Eqs. 2, 3).

In Fig. 5, the dependence of  $\lambda_D$  on the local outer scale Reynolds number  $Re_\delta$  is shown. The curve was compiled by dividing the Reynolds number range 3200 to 8400 into 26 bins, then computing the thicknesses for each bin as above, with the same threshold and connectivity conditions. The curve thus represents the average layer thickness for the given  $Re_\delta$ . The dashed line in the plot is the curve  $14.5 \cdot Re_\delta^{-3/4}$ . The actual least-squares fit gives a Reynolds number dependence of  $Re_\delta^{-.74}$ . From this plot it is quite evident that the *average* layer thicknesses observe the  $Re_\delta^{-3/4}$  Batchelor scaling. (The constant  $\Lambda = 14.5$  differs slightly from that found from the curve of Fig. 4 because the data are not evenly distributed in  $Re_\delta$  space.)

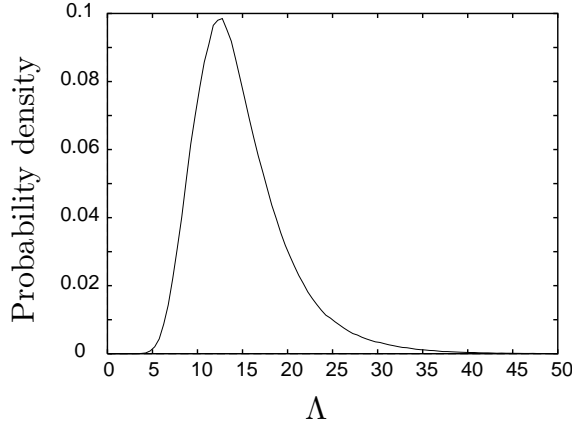


FIGURE 4. Distribution of dissipation layer thicknesses, expressed in terms of  $\Lambda$ .

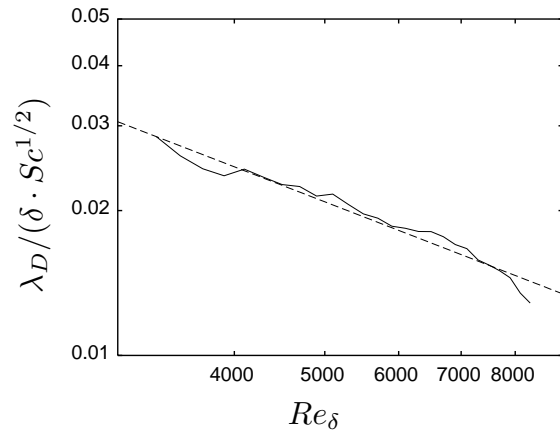


FIGURE 5. Average layer thickness conditioned on local outer scale Reynolds number. Current data, — ;  $14.5 \cdot Re_\delta^{-3/4}$ , - - - .

However, Dowling (1991) concluded that while the majority of the dissipation occurred at scales which followed Batchelor scaling, a substantial portion of the dissipation, in particular the highest local dissipation values, occurred at the larger Taylor scales. With the present data this can be assessed by considering the Reynolds number dependence of the extremes of the thickness distribution. Figure 6 shows the  $Re_\delta$  dependence of the average thickness of the thickest and thinnest 25% of layers, together with the overall average as shown in Fig. 5. There is no evidence of Taylor scaling of the thickest layers. The least-squares fit to the thickness curve for the thickest 25% of the layers has dependence  $Re_\delta^{-.73}$ , while the curve for the thinnest 25% has dependence  $Re_\delta^{-.75}$ . The trend of weaker  $Re_\delta$  dependence for thicker layers is consistent with Dowling's hypothesis, but this very slight difference of  $Re_\delta^{-.73}$  versus  $Re_\delta^{-.75}$  is likely within experimental tolerances, and certainly gives no indication of  $Re_\delta^{-1/2}$  scaling.

Figure 7 shows the dependence of  $\Lambda$  on the threshold value of the dissipation rate. Again, in contradiction to the idea that high dissipation values take place on length

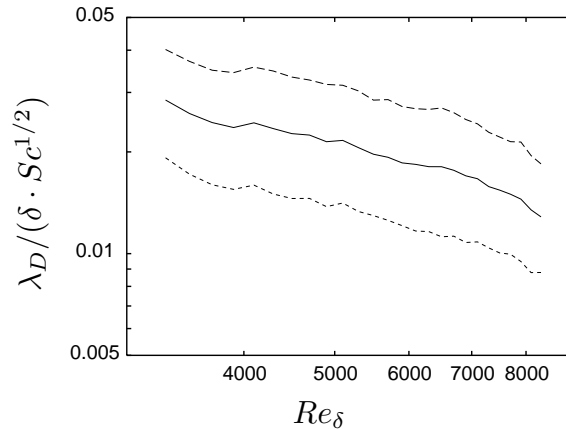


FIGURE 6. Layer thickness conditioned on  $Re_\delta$ . Average thickness of all layers, — ; average of thickest 25% of layers, - - - ; average of thinnest 25%, ····· .

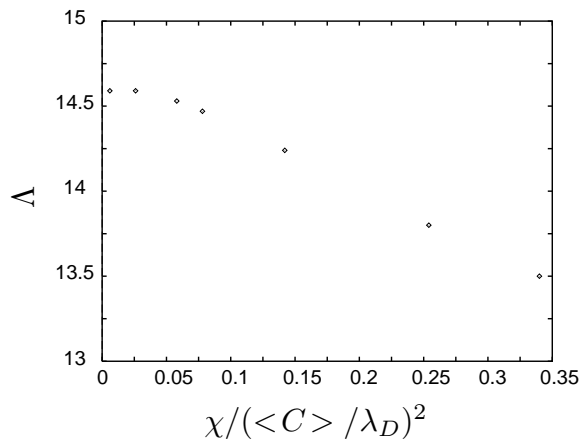


FIGURE 7. Dependence of the coefficient  $\Lambda$  on the threshold value of the dissipation rate.

scales observing Taylor scaling, it can be seen that higher values of  $\chi$  are associated with *thinner* layers.

### 2.2.2 Dissipation rate scaling

The scaling of mean scalar dissipation rates with downstream distance in turbulent jets is of interest in certain models of the stabilization properties of turbulent jet diffusion flames. Peters & Williams (1983) suggest that the mean scalar dissipation rate should scale linearly with the global strain rate, with the square of the local mean centerline scalar concentration, and with the inverse square of the local jet width. For the planar turbulent jet, we thus expect  $\chi \propto (U_0/h)(y/h)^{-3}$ . The few existing measurements for the downstream dependence of the mean dissipation fail to observe the expected scalings, however. In round jets, both Lockwood & Moneib (1980) and Effelsberg & Peters (1988) found that the decay of  $\chi$  in the self-similar region was significantly weaker than the predicted  $(y/d)^{-4}$  dependence.

The present measurements span from 65 to 127 jet widths downstream, and

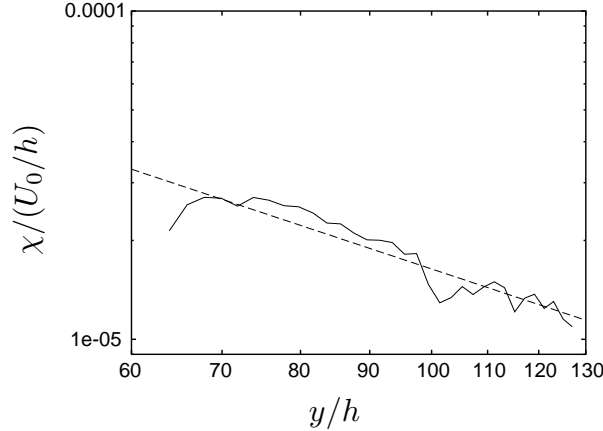


FIGURE 8. Downstream decay of scalar dissipation rate, normalized by global strain rate. Current data, — ; best fit,  $y^{-1.4}$ , ---- .

so can provide useful information on the decay of the dissipation rate. However, because the present measurements were intended primarily for investigation of the structure of the scalar dissipation rate field, no direct effort was made to correlate the measured scalar concentrations to the initial jet value. We account for the scalar decay here by assuming that the recommended scaling from Chen & Rodi (1980) applies, namely

$$\langle C(y) \rangle / C_0 = 2.46 (y/h)^{-1/2},$$

where  $\langle C(y) \rangle$  and  $C_0$  are the local mean centerline concentration and initial jet concentration, respectively, and the effect of the jet and ambient fluid density difference has been included. For each data set of 15 or 30 image pairs, the centerline average is found, the effective  $C_0$  value is computed from the above formula, and this  $C_0$  is then used to normalize the scalar field values for the purpose of compiling the dimensional dissipation rate  $\chi$ .

Figure 8 shows the conditional average of  $\chi/(U_0/h)$  with downstream distance, for off-center positions  $|x|/\delta \leq 0.05$ , i.e. near the centerline. The dissipation rate  $\chi$  is computed here as  $\chi = D (\partial C/\partial x_i)(\partial C/\partial x_i)$ , where  $D$  is the propane-air diffusivity,  $0.114 \text{ cm}^2/\text{s}$ ,  $C$  is the scalar concentration normalized by  $C_0$ , and the  $x_i$  are dimensional. The global strain rate  $U_0/h$  has been divided from  $\chi$  to isolate the dependence of the decay on  $(y/h)$ . The dotted line is the best linear fit to the data, which has a slope of -1.4. Consistent with previous results, the data predict a much slower decay than anticipated by the theory of Peters & Williams (1983). It should be pointed out that for both planar and round jets, the fine scales increase in size with downstream distance, and thus resolution requirements are relaxed as the measurement area moves away from the nozzle. It is therefore possible that the decay rates are underestimated because high dissipation rates are more accurately measured further downstream. For the present measurements, however, the relative resolution differs at most by a factor of two between the  $y = 65h$  and  $y = 127h$  locations. Considering only these two locations, a dependence of  $\chi$  on  $y^{-3}$  would require that  $\chi$  decay by a factor of 7.5 from  $y = 65h$  to  $127h$ , while the measured

$y^{-1.4}$  dependence corresponds to a  $\chi$  decay factor of 2.5. From the evidence of existing measurements which assess the effects of varying resolution (e.g. Dowling (1991), Antonia & Mi (1993)), this factor of three discrepancy cannot be accounted for by the resolution difference between near and far downstream positions. Rather it appears, based on these limited results, that the current understanding of the scaling of dissipation rates is quite incomplete.

### 3. Future plans

While this paper has focused on the fine scales of the mixing field, the data are also well suited to analysis of larger scale properties and, perhaps more significantly, to analysis of the interactions of the large and small scales. At the upstream limit of the measurement domain,  $y = 65h$ , the jet width (Eq. 4) is  $\delta \approx 25h$ , while at the downstream limit,  $y = 127h$ , we find that the jet width is  $\delta \approx 50h$ . Since each imaging plane spans  $34h$ , each scalar field image covers a range of scales from the finest mixing scale to in excess of  $0.68\delta$ . It is therefore possible, for example, to investigate scale similarity over the full range of flow length scales. As pointed out by Frederiksen *et al.* (1996), information on the full three-dimensional dissipation rate is necessary to assess the true scale similarity of the mixing process. Direct, *a priori* assessments of subgrid models for LES can also be performed, by filtering the scalar and scalar dissipation results and comparing the model predictions based on these filtered quantities with the actual values on the original, resolved measurement grid. Similar tests have been demonstrated both on DNS data for  $Sc = 1$  mixing, and on experimental liquid-phase mixing results (Cook & Riley (1994)).

## REFERENCES

- ANTONIA, R. A. & MI, J. 1993 Temperature dissipation in a turbulent round jet. *J. Fluid Mech.* **280**, 179-197.
- BATCHELOR, G. K. 1952 The effect of homogeneous turbulence on material lines and surfaces. *Proc. Roy. Soc. London A.* **213**, 349-366.
- BRADBURY, L. J. S. 1965 The structure of a self-preserving turbulent plane jet. *J. Fluid Mech.* **23**, 31-64.
- BUCH, K. A. & DAHM, W. J. A. 1991 Fine scale structure of conserved scalar mixing in turbulent shear flows:  $Sc \gg 1$ ,  $Sc \approx 1$  and implications for reacting flows. *Report 026779-5*, University of Michigan.
- CHEN, C. J. & RODI, W. 1980 *Vertical Turbulent Buoyant Jets: A Review of Experimental Data*. Pergamon.
- COOK, A. W. & RILEY, J. J. 1994 A subgrid model for equilibrium chemistry in turbulent flows. *Phys. Fluids* **6**, 2868-2870.
- DOWLING, D. R. 1991 The estimated scalar dissipation rate in gas-phase turbulent jets. *Phys. Fluids A* **3**, 2229-2246.
- DOWLING, D. R. & DIMOTAKIS, P. E. 1990 Similarity of the concentration field of gas-phase turbulent jets. *J. Fluid Mech.* **218**, 109-141.

- EFFELSBERG, E. & PETERS, N. 1988 Scalar dissipation rates in turbulent jets and jet diffusion flames. In *Proc. Twenty-Second Symp. (Int'l) on Combustion*, 693-700.
- ESWARAN, V. & POPE, S. B. 1988 Direct numerical simulations of the turbulent mixing of a passive scalar. *Phys. Fluids* **31**, 506-520.
- EVERITT, K. W. & ROBINS, A. G. 1978 The development and structure of turbulent plane jets. *J. Fluid Mech.* **88**, 563-583.
- FEIKEMA, D. A., EVEREST, D. & DRISCOLL, J. F. 1996 Images of dissipation layers to quantify mixing within a turbulent jet. *AIAA J.* **34**, 2531-2538.
- FREDERIKSEN, R. D., DAHM, W. J. A. & DOWLING, D. R. 1996 Experimental assessment of fractal scale similarity in turbulent flows. Part I: One-dimensional intersections. *J. Fluid Mech.* **327**, 35-72.
- FRIEHE, C. A., VAN ATTA, C. W. & GIBSON, C. H. 1971 Jet turbulence: dissipation rate measurements and correlations. In *AGARD Turbulent Shear Flows*, **CP-93**, 18-1-18-7.
- LOCKWOOD, F. & MONEIB, H. 1980 Fluctuating temperature measurements in a heated round free jet. *Comb. Sci. Tech.* **22**, 63-81.
- NAMAZIAN, M., SCHEFER, R. W. & KELLY, J. 1988 Scalar dissipation measurements in the developing region of a jet. *Comb. Flame* **74**, 147-160.
- PAUL, P., VAN CRUYNINGEN, I., HANSON, R. K. & KYCHAKOFF, G. 1990 High resolution digital flowfield imaging of jets. *Exp. Fluids* **9**, 241-250.
- PETERS, N. 1983 Local quenching due to flame stretch and non-premixed turbulent combustion. *Comb. Sci. Tech.* **30**, 1-17.
- PETERS, N. & WILLIAMS, F. A. 1983 Liftoff characteristics of turbulent jet diffusion flames. *AIAA J.* **21**, 423-429.
- SOUTHERLAND, K. B. & DAHM, W. J. A. 1994 A four-dimensional experimental study of conserved scalar mixing in turbulent flows. *Report 026779-12*, University of Michigan.
- SU, L. K. & CLEMENS, N. T. 1998a The structure of the three-dimensional scalar gradient in gas-phase turbulent jets. *AIAA Paper 98-0429*.
- SU, L. K. & CLEMENS, N. T. 1998b Planar measurements of the full three-dimensional scalar dissipation rate in gas-phase turbulent flows. Submitted to *Exp. Fluids*.
- TENNEKES, H. & LUMLEY, J. L. 1972 *A First Course in Turbulence*. MIT Press.
- VINCENT, A. & MENEGUZZI, M. 1991 The spatial structure and statistical properties of homogeneous turbulence. *J. Fluid Mech.* **225**, 1-20.
- YIP, B. & LONG, M. B. 1986 Instantaneous planar measurement of the complete three-dimensional scalar gradient in a turbulent jet. *Opt. Lett.* **11**, 64-66.
- YIP, B., SCHMITT, R. L. & LONG, M. B. 1988 Instantaneous three-dimensional concentration measurements in turbulent jets and flames. *Opt. Lett.* **13**, 96-98.